Journal of Ceramic Processing Research. Vol. 24, No. 4, pp. 693~699 (2023)
(Received 24 April 2023, Received in revised form 4 August 2023, Accepted 7 August 2023)
https://doi.org/10.36410/jcpr.2023.24.4.693

J O U R N A L O F
Ceramic Processing Research

Regulation of $BaTiO_3$ ceramics' electrical properties by varying $Na_{0.5}Bi_{0.5}TiO_3$ dopants

Shuiyun Li[a], Mingyang Ma[a], Yongshang Tian[a,*], Ruobing Li[a], Xiongjie Hu[b] and Peng Liu[a]
[a]*College of Chemistry and Chemical Engineering, Henan Key Laboratory of Utilization of Non-Metallic Mineral in the South of Henan, Xinyang Normal University, Xinyang 464000, China*
[b]*Loyalty Enterprise Development (Xinyang) Co., LTd., Xinyang 464017, China*

The piezoelectricity of $BaTiO_3$ (BT) ceramics could be effectively regulated by $Na_{0.5}Bi_{0.5}TiO_3$ (NBT) compounds, and the mechanism is still controversial. In this work, BT-*x*NBT ceramics with various NBT contents (*x*) were synthesized by a conventional solid-state sintering process. The characteristic of phase, cross-section morphology, permittivity, ferroelectricity, and piezoelectricity were fully explored by some advanced test equipment. With an increment of *x*, the ceramics possessed a high densification with a sole tetragonal phase, the diffused phase transition and relaxor ferroelectricity enhanced firstly and then receded. The inherent ferroelectricity and large strain of NBT materials under an electric field were deemed as the reasons for the increased ferroelectricity and piezoelectric coefficients with excessive *x*, respectively. Moreover, influences of impurity phases, fine grains, internal stress, etc. on the electrical properties were also discussed. This work provides a novel strategy to regulate BT-based lead-free piezoelectric ceramics.

Keywords: BT ceramics, NBT dopants, Tetragonal phase, Relaxor ferroelectricity, Piezoelectric coefficients.

Introduction

Piezoceramic material is the most fundamental for electromechanical devices, which could accomplish the aim of electrical-mechanical energy interconversion [1]. The toxicity of lead zirconate titanate (PZT) based piezoceramic materials are banned to use by the regulations, though they feature excellent electrical properties [2, 3]. Some attractive classes of lead-free piezoceramic materials were developed for the substitution [4-6]. Among the lead-free piezoceramic materials, barium titanate ($BaTiO_3$, BT) was once considered a serious potential candidate since it was the first discovered polycrystalline piezoceramic material and might feature excellent electrical properties [7, 8]. However, BT ceramics possessed a low Curie temperature (T_C) of 120 °C, low piezoelectricity, and low electric field-induced strains, which diminished the researchers' interest.

BT lead-free ceramics was confirmed to have comparable piezoelectricity to PZT ceramics by Ca and Zr co-doping in the structure in 2009, which aroused widespread attention [9]. Since then, their limited low-temperature range stability was fully researched for their potential actual application. Chemically modifying and microstructurally engineering are the most common methods in BT-based materials [10-12], while the T_C was not significantly improved. Moreover, the electric field-induced piezoelectric coefficients were not highly elevated. Thus, some dopants of compounds with high T_C and excellent piezoelectric coefficients were taken into account for optimizing their inherent imperfection. For example, Chaudhary et al. studied bismuth ferrite ($BiFeO_3$) doped BT ceramics, which exhibited a high T_C of 400-500 °C and excellent insulation properties [13]. Singh et al. observed phase evolution from orthorhombic towards tetragonal in potassium sodium niobate ($K_{0.5}Na_{0.5}NbO_3$, KNN) doped BT ceramics, showing excellent electrical properties assessed with suitable KNN contents [14]. Lv et al. reported bismuth sodium titanate ($Na_{0.5}Bi_{0.5}TiO_3$, NBT) doped BT ceramics, which exhibited ideal ferroelectric properties and high T_C [15]. From the mentioned results above, the strategies to improve BT-based ceramics piezoelectric properties were a certain effect. Among the research, the NBT dopants in BT-based ceramics attracted our team's attention because the mechanism of electrical properties improvement is still controversial. For example, viewpoints of phase transformation [16], antiferroelectric-ferroelectric phase transition [17], nonergodic relaxor state [18], relaxor ferroelectricity [19], etc. were respectively concentrated on and discussed largely. Therefore, exploring the exact mechanism behind the improved electrical properties is essential for the BT-BNT materials on electromechanical device

*Corresponding author:
Tel : +86 0376 6390702
Fax: +86 0376 6390702
E-mail: tianyongshang423@163.com; tianyongshang@xynu.edu.cn

applications.

In this work, the influences of impurity phases, fine grains, and internal stress on permittivity, relaxor ferroelectricity, and piezoelectricity of the BT-*x*NBT ceramics with various NBT contents were investigated emphatically. With the phase information at room temperature and the permittivity results, we assumed that there was no phase transition in the BT-*x*NBT ceramics. Additionally, the elevated ferroelectricity and piezoelectric coefficients that was related to the inherent performance of NBT materials were also discussed.

Experimental Procedure

Preparation procedure

Lead-free ceramics with a stoichiometric mole of $(1-x)BaTiO_3$-$xNa_{0.5}Bi_{0.5}TiO_3$ (abbreviated as BT-*x*NBT, x = 0, 0.04, 0.08, 0.12, and 0.16) were prepared by a conventional solid-state reaction method in four stages, using analytic reagents of $BaCO_3$, TiO_2, Na_2CO_3, and Bi_2O_3 nanopowders as the raw materials. Firstly, the nanopowders were milled in a planetary ball mill using agate ball media with ethanol as a dispersion for 15 h after accurate weighing was done. The powders were dried at 120 °C for 2 h and calcined at 870 °C for 4 h in a muffle furnace, then the calcined powders were reground and re-calcined similar to the above-stated procedure for the BT-*x*NBT powders. Secondly, the BT-*x*NBT powders were pressed into a disk of diameter 15 mm under a uniaxial pressure of 25 MPa for compacted pellets after they were mixed with a polyvinyl alcohol solution (5 wt.%) as a binder. Thirdly, the compacted pellets were buried in self-sourced sacrificial powder and sintered at 1090-1250 °C for 4 h in air atmosphere for the BT-*x*NBT ceramics. Lastly, the ceramics were polished and coated on silver electrodes for investigating the following electrical performance.

Measurement and characterization

The phase identification of the BT-*x*NBT ceramics was confirmed by X-ray powder diffraction (XRD; SmartLab 9k, Japan) with Cu-Kα radiation after the ceramics were crashed for powder in an agate mortar. The density was determined by Archimedes' immersion method. Field emission scanning electron microscopy (SEM; S4800, Japan) was applied to measure the fractured morphology. Temperature- and frequency-dependent relative permittivities (ε_r) and loss tangents (tan δ) were tested using an impedance analyzer (WK-65120B, U.K.). The polarisation-electric field hysteresis loops were characterized by a ferroelectric evaluation system (RTI-Multiferroic II, U.S.A.) at a frequency of 10 Hz, and an optical reflectance sensor (MTI-2100, U.S.A.) was used to calculate the piezoelectric coefficients (d_{33}*). A quasi-static piezoelectric constant testing meter (ZJ-3AN, China) was carried out to detect the piezoelectric constant (d_{33}) after the ceramics were poled under a direct current (dc) electric field of 30-40 kV/cm for 50 min in silicon oil bath [20]. A precision impedance analyzer (E4990A, U.S.A.) was used to study the planar vibration electromechanical coupling (k_p) and mechanical quality (Q_m) factors by resonance-antiresonance method at ambient temperature.

Results and Discussion

Fig. 1 displays XRD patterns of the BT-*x*NBT ceramics prepared with different NBT contents (x). The main diffraction peaks in Fig. 1(a) could be indexed to PDF no. 05-0626, suggesting the ceramics possessed a tetragonal phase. A pure perovskite (ABO_3) structure could be observed with a small addition of x (< 0.08), suggesting the compounds of NBT could form a stable solid solution with BT, since they both have a similar ABO_3 structure. However, minimal traces of impure diffraction peaks could be found at 2θ around 30° and 44° when x > 0.12, because the solid solubility limit of the ABO_3 lattice, and the impurity phases might be inferred as $BaTi_2O_5$ (PDF no. 70-1188) and $Ba_6Ti_{17}O_{40}$ (PDF no. 77-1566) [21, 22]. The enlarged view in Fig. 1(b) could apparently show the characteristic (002) and (200) diffraction peaks of the tetragonal phase, and the relative intensity ratio of the (200)/(002) peak was almost 2. The results also indicated NBT dopants could not give rise to the phase evolution with the doping range in this study. From the Fig. 1(b), it could be seen the (002) and (200) diffraction peaks shifted towards higher 2θ angles direction with increasing addition of NBT contents, which was attributed to the shrunken crystalline interplanar spacing from the Bragg equation ($2d\sin\theta = n\lambda$) [21, 23]. The shrunken crystalline interplanar spacing could be derived from the substitute of Ba^{2+} (0.161 nm) by the smaller Na^+ (0.097 nm)/Bi^{3+}

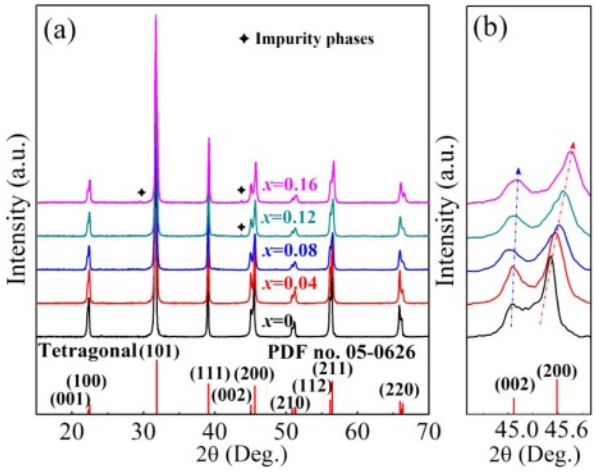

Fig. 1. (a) XRD patterns (2θ = 15-70°) and (b) selected enlarged regions (2θ = 44.5-46.0°) of the BT-*x*NBT ceramics prepared with different NBT contents (x).

Table 1. Lattice parameters of the BT-*x*NBT ceramics prepared with different NBT contents (*x*).

x	*a* (Å)	*b* (Å)	*c* (Å)	*Axial angle* (°)
0	3.994(1)	3.994(1)	4.038(2)	90
0.04	3.933(5)	3.933(5)	3.976(4)	90
0.08	3.875(1)	3.875(1)	3.917(9)	90
0.12	3.818(6)	3.818(6)	3.860(7)	90
0.16	3.762(3)	3.762(3)	3.804(8)	90

(0.096 nm) in the structure, and the analysis is in line with the refined lattice parameters results that were calculated by a Rietveld fitting procedure listed in Table 1. Additionally, the intensity of (200) and (002) diffraction peaks decreased with an increment of NBT contents, showing the crystallinity of the ceramics weakened.

The density (ρ) and relative density (ρ_r) of the BT-*x*NBT ceramics assessed with different NBT contents (*x*) are shown in Fig. 2. It could be observed ρ_r of the ceramics featured a big value (~96%-~98%), showing the ceramics had a high densification. The density went down with an increment of NBT contents, because the theoretical density of NBT (5.934 g/cm^3) was virtually lower than BT (6.012 g/cm^3). The cross-section morphology of the BT-*x*NBT ceramics with various NBT contents (*x*), which could exhibit the message of densification and grain size, are shown in Fig. 3. From the figure, little cavities were found, indicating high densification of the ceramics. The average grain size, which was calculated by a linear intercept method, decreased from 1.85 μm to 1.26 μm with the increasing addition of *x* [24]. The decreased average grain size was due to the formed fine grains in the structure. Moreover, the grains for all the ceramics possessed

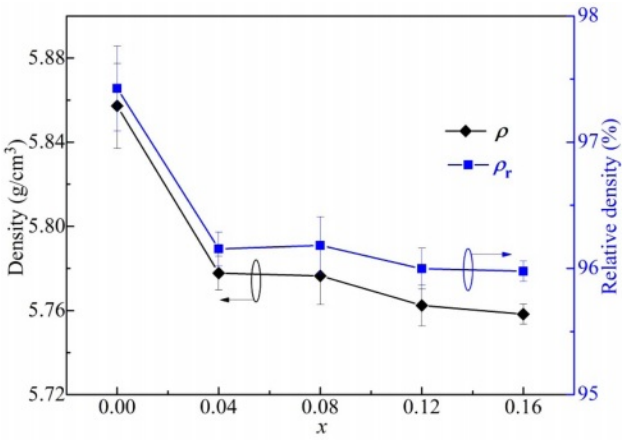

Fig. 2. The density (ρ) and relative density (ρ_r) of the BT-*x*NBT ceramics prepared with different NBT contents (*x*).

square structures obviously, because the ceramics featured a tetragonal phase as mentioned in Fig. 1.

Fig. 4 displays the temperature-dependent relative permittivities (ε_r) and loss tangents (tan δ) of the BT-*x*NBT ceramics measured at 10 kHz. It can be seen two apparent permittivity peaks around ~120 and ~180 °C (except the BT-*x*NBT ceramic when $x = 0$) corresponded to thermally-induced ferroelectric to the relaxor transition temperature (T_{F-R}) and Curie temperature (T_C), respectively [25]. The T_C increased from 116 °C to 178 °C monotonously with an increment of NBT contents, suggesting NBT dopants could improve the value of T_C effectively. There existed only a tetragonal phase at an ambient temperature according to the XRD results in Fig. 1, it could be deduced that there was no phase transition around T_{F-R} of the BT-*x*NBT ceramics. The T_C peak broadened monotonously with an increment of *x* basically, showing the diffused phase transition

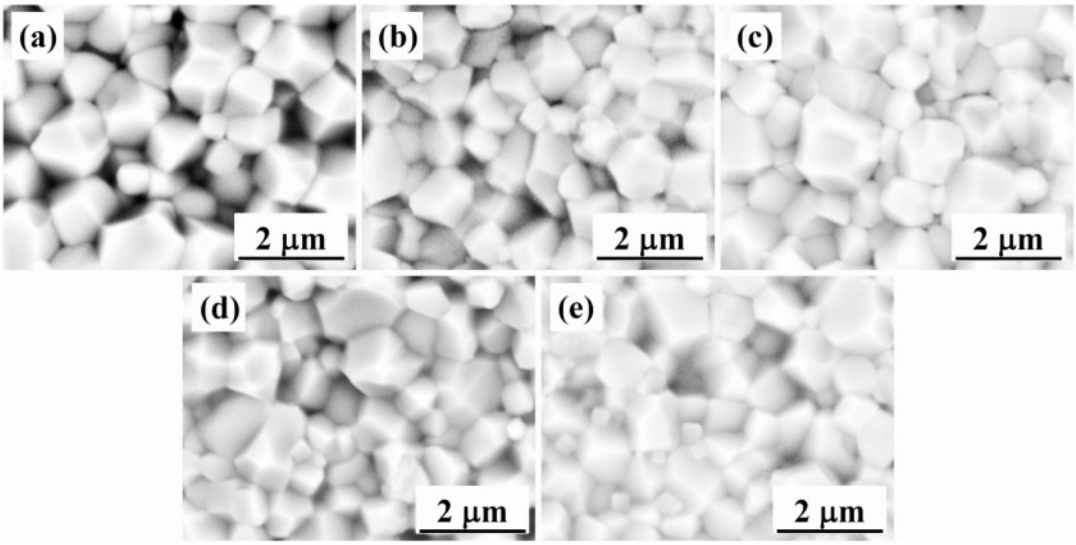

Fig. 3. SEM micrographs for the cross-section morphology of the BT-*x*NBT ceramics prepared with different NBT contents (*x*): (a) 0, (b) 0.04, (c) 0.08, (d) 0.12, and (f) 0.16.

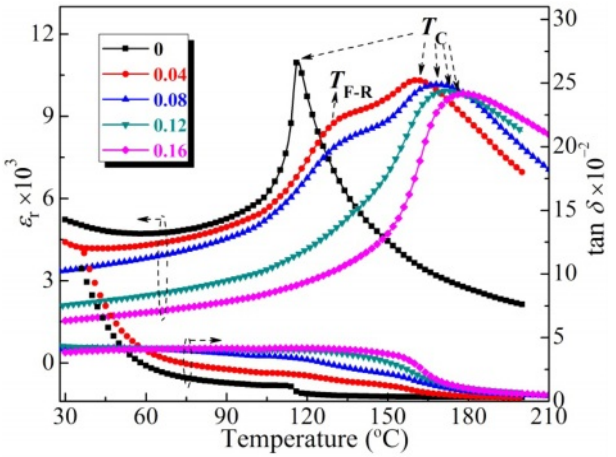

Fig. 4. Temperature-dependent relative permittivities (ε_r) and loss tangents (tan δ) of the BT-xNBT ceramics measured at 10 kHz.

(DPT) behavior enhanced [26, 27]. The tan δ around T_C elevated with an increment of x, which was due to the compositional fluctuations and the formed fine grains in the structure with excessive NBT contents. Additionally, the ceramics possessed small tan δ values, which could be associated with subtle structural defects and highly densified structure [28].

The relative permittivities (ε_r) and loss tangents (tan δ) of the BT-xNBT ceramics with various NBT contents (x) measured at various frequencies (100 Hz-50 kHz) are shown in Fig. 5. It could be seen the dielectric dispersion enhanced first and then deteriorated with an increment of NBT contents, implying the relaxor behaviour initially elevated and then decreased. The loss tangents peaks represented to T_{F-R} and T_C could be also detected in Fig. 5, and they were relatively lower than the temperature corresponded to

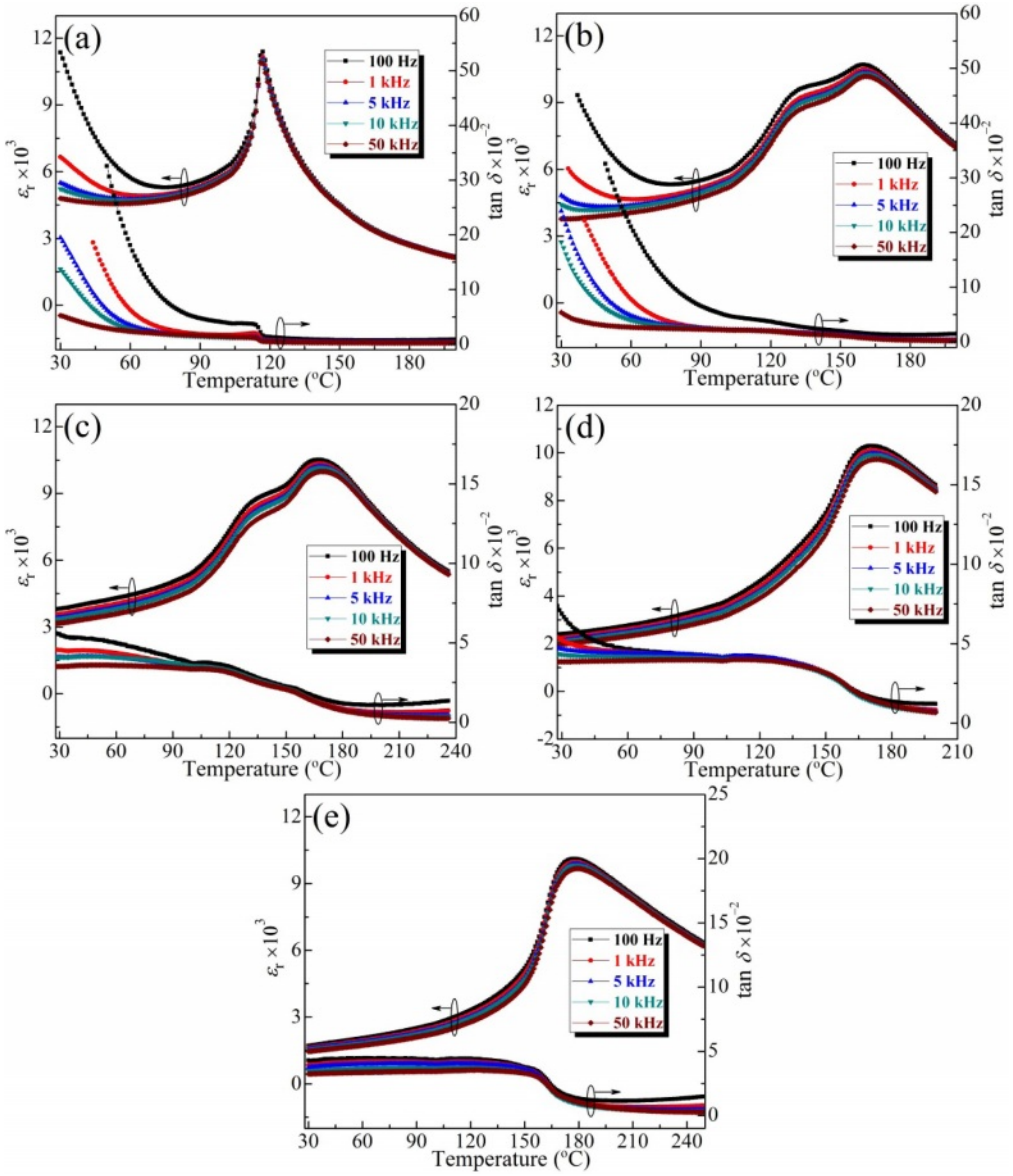

Fig. 5. The relative permittivities (ε_r) and loss tangents (tan δ) of the BT-xNBT ceramics with various NBT contents (x): (a) 0, (b) 0.04, (c) 0.08, (d) 0.12, and (f) 0.16 measured at various frequencies (100 Hz-50 kHz).

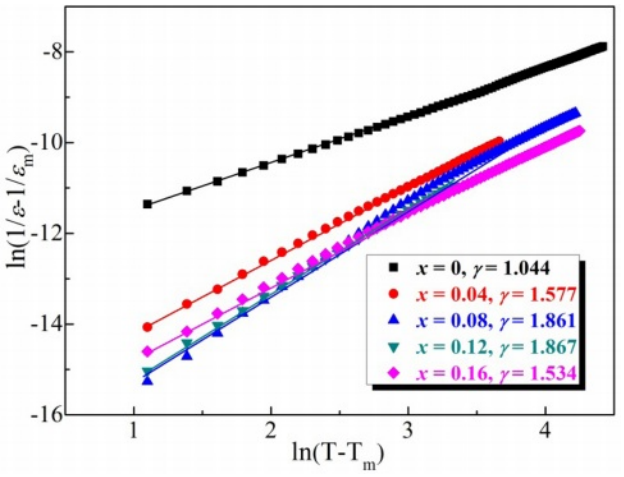

Fig. 6. $\ln(T - T_m)$ dependent $\ln(1/\varepsilon_r - 1/\varepsilon_m)$ of the BT-xNBT ceramics assessed at a frequency of 10 kHz.

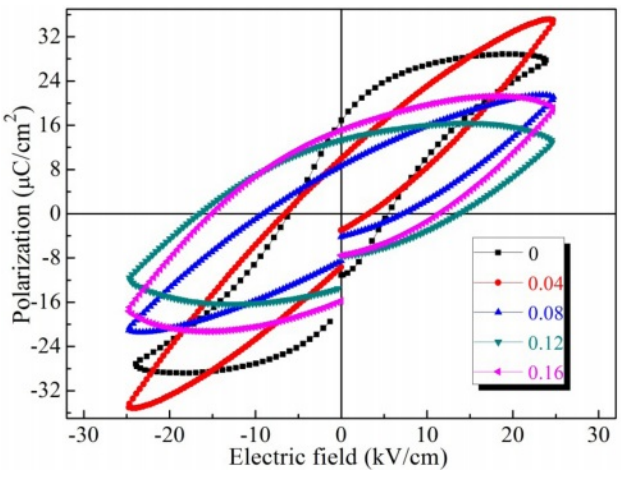

Fig. 7. Polarisation-electric field (*P-E*) hysteresis loops of the BT-xNBT ceramics tested at 10 Hz at ambient temperature.

permittivity peaks, because the orientation of the dipoles would take a certain amount of time [29], that is the same reason for the various permittivity peaks under different frequency. At a low frequency, the diploes have enough time for reaching the balanced state, and the permittivity peaks would appear early. Moreover, the increased T_C was also attributed to the restrained diploes on the crystal surface assessed at a high frequency [30].

Fig. 6 displays $\ln(T - T_m)$ dependent $\ln(1/\varepsilon_r - 1/\varepsilon_m)$ of the BT-xNBT ceramics assessed at a frequency of 10 kHz. The figure was introduced for revealing the quantitative diffuseness exponent (γ) for the BT-xNBT ceramics, which was investigated by the optimized Curie–Weiss law in Eq. (1).

$$\ln\left(\frac{1}{\varepsilon_r}-\frac{1}{\varepsilon_m}\right) = \gamma\ln(T-T_m)-\ln C' \quad (1)$$

where T_m is the temperature corresponding to the maximum permittivity (ε_m), and C' represents the optimized Curie-Weiss constant. The fitted γ value would theoretically range from 2 (typical relaxor ferroelectric) to 1 (normal ferroelectric). It could be found, the diffuseness exponent increased from 1.044 to 1.867 with an increment of NBT contents from 0 to 0.12, indicating the relaxor ferroelectric behavior enhanced. Then, the γ decreased to 1.534 when increasing NBT contents further, interpreting the ferroelectric strengthened with excessive NBT contents. The enhanced relaxor ferroelectricity could be ascribed to the large local compositional fluctuation or electron scattering in the fine grains [31], while the receded relaxor ferroelectricity when $x > 0.16$ might be associated with the relatively better inherent ferroelectricity of NBT mainly [32].

Polarisation-electric field (*P-E*) hysteresis loops of the BT-xNBT ceramics that was tested at 10 Hz at ambient temperature are shown in Fig. 7. It could be observed, the ceramics possessed typical ferroelectric hysteresis loops when $x = 0$, while the ceramics had large leakage current when doping with NBT contents. The enhanced leakage current with excessive x might be due to the compositional disorder and the large electron scattering in the structure [33]. With an increment of x, the remnant polarization (P_r) decreased initially and then increased, suggesting the ferroelectricity abruptly deteriorated firstly and then slightly elevated. However, the coercive field (E_c) featured an opposite tendency to various P_r, which was due to the strong clamping effect of the domain wall with fine grains or large local compositional fluctuation when $x < 0.12$ [31, 34]. The slightly decreased E_c was might be due to many NBT components dopants in the structure when $x = 0.16$, a similar explanation was consistent with the

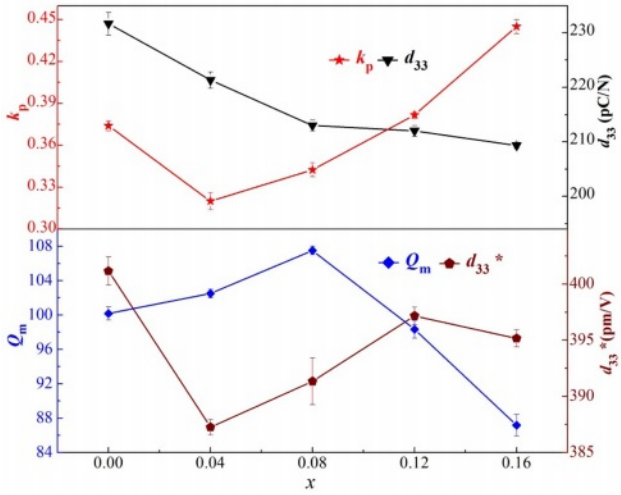

Fig. 8. The variations of planar vibration electromechanical coupling factors (k_p), mechanical quality factor (Q_m), piezoelectric constant (d_{33}), and the calculated piezoelectric coefficients (d_{33}*) of the BT-xNBT ceramics prepared with varying NBT contents (x).

results in Fig. 6. Moreover, the impurity phases would also lead to the receded ferroelectricity, because of the hindered influence on the switch of dipoles [35].

The variations of planar vibration electromechanical coupling factors (k_p), mechanical quality factor (Q_m), piezoelectric constant (d_{33}), and the calculated piezoelectric coefficients (d_{33}*) of the BT-xNBT ceramics prepared with varying NBT contents (x) are displayed in Fig. 8. It could be found k_p firstly decreased and then increased with increasing addition of x, while d_{33} kept decreasing over the doping range. With a small amount of NBT contents ($x < 0.04$), the deteriorated piezoelectricity was due to the large internal stress with local compositional fluctuation [36]. Besides, the receded d_{33} with further increased x was due to the formed fine grains and the impurity phases [37]. Moreover, the higher electronegative Bi^{3+} (2.02)/Na^{+} (0.93) ions substituted to the Ba^{2+} (0.89) ions in the structure was deemed as the main reason for the increased k_p when $x > 0.04$ [38]. The Q_m possessed an opposite trend to k_p, while the d_{33}* had a similar results to d_{33}, those results were derived from the inherent high strain under an electric field of NBT. A little decreased d_{33}* of the BT-xNBT ceramics was found when $x = 0.16$, which was associated with the enhanced pinching effect of domain walls because of the small grains and impurity phases [39].

Conclusions

Lead-free BT-xNBT ceramics were successfully prepared by a conventional solid-state sintering process. Various NBT contents (x) would not promote the tetragonal phase evolution, while they could influence the electrical properties apparently. The subtle structural defects and highly densified structure were in favor of decreasing the dielectric loss. The small grain size and the impurity phases would appear with excessive x, bringing about the enhanced relaxor ferroelectricity and deteriorated piezoelectricity, while the slightly enhanced electrical properties were found when $x = 0.16$ was due to the inherent characteristic of NBT. The results of piezoelectric coefficients (d_{33}*) with an increment of x was not consistent with the piezoelectric constant (d_{33}), because the NBT featured a relatively larger strain under an electric field than that of BT. The results in this study could reflect the relationship of the electrical properties of BT ceramics assessed with various NBT contents, and provide a new thought to optimize the BT materials.

Acknowledgements

This work was financially supported by the Henan Province Science and Technology Research Project (222102230024), National Natural Science Foundation of China (51902279), and the Key Youth Scholar Funding Project of Henan Province of China (2021GGJS097). The authors also would like to thank the Analysis & Testing Center of XYNU for their testing help.

References

1. J. Rödel, K.G. Webber, R. Dittmer, W. Jo, M. Kimura, and D. Damjanovic, J. Eur. Ceram. Soc. 35 (2015) 1659-1681.
2. E. Cross, Nature 432 (2004) 24-25.
3. T.R. Shrout and S.J. Zhang, J. Electroceram. 19 (2007) 113-126.
4. X. Zhou, G. Xue, H. Luo, C.R. Bowen, and D. Zhang, Prog. Mater. Sci. 122 (2021) 100836.
5. T. Takenaka and H. Nagata, J. Eur. Ceram. Soc. 25 (2005) 2693-2700.
6. T. Zheng, J. Wu, D. Xiao, and J. Zhu, Prog. Mater. Sci. 98 (2018) 552-624.
7. H. Jaffe, Ind. Eng. Chem. 42[2] (1950) 264-268.
8. G.H. Haertling, J. Am. Ceram. Soc. 82[4] (1999) 797-818.
9. W. Liu and X. Ren, Phys. Rev. Lett. 103 (2009) 257602.
10. D.C. Sinclair and J.P. Attfield, Chem. Commun. 0 (1999) 1497-1498.
11. L. Ben and D.C. Sinclair, Appl. Phys. Lett. 98 (2011) 092907.
12. M. Acosta, N. Novak, V. Rojas, S. Patel, R. Vaish, J. Koruza1, G.A. Rossetti Jr., and J. Rödel, Appl. Phys. Rev. 4 (2017) 041305.
13. P. Chaudhary, R. Shukla, S. Dabas, and O.P. Thakur, J. Alloy. Compd. 869 (2021) 159228.
14. R. Singh, K. Kambale, A.R. Kulkarni, and C.S. Harendranath, Mater. Chem. Phys. 138[2-3] (2013) 905-908.
15. J. Lv, Q. Li, Y. Li, M. Tang, D. Jin, Y. Yan, B. Fan, L. Jin, and G. Liu, Chem. Eng. J. 420 (2021) 129900
16. T. Takenaka, K.I. Maruyama, and K. Sakata, Jpn. J. Appl. Phys. 30 (1991) 2236-2239.
17. B.N. Rao, R. Datta, S.S. Chandrashekaran, D.K. Mishra, V. Sathe, A. Senyshyn, and R. Ranjan, Phys. Rev. B, 88 (2013) 224103.
18. H. Liu, C. Zhou, J. Chen, C. Yuan, S. Cheng, J. Xu, Q. Li, G. Chen, and G. Rao, Ceram. Int. 49[4] (2023) 6332-6342.
19. Y. Jia, H. Fan, A. Zhang, H. Wang, L. Lei, Q. Quan, G. Dong, W. Wang, and Q. Li, J. Eur. Ceram. Soc. 43[3] (2023) 947-956.
20. Y. Tian, L. Cao, S. Li, Q. Wu, and Q. Jing, J. Xinyang Norm. Univ. (Nat. Sci. Ed.) 34 (2021) 467-471.
21. T.A. Jain, K.Z. Fung, and J. Chan, J. Alloy. Compd. 468[1-2] (2009) 370-374.
22. C. Lee, K.J. Lee, H.G. Kim, S.H. Lim, M.S.V. Kumar, S. Yoda, and W.S. Cho, J. Ceram. Process. Res. 17[2] (2016) 97-102.
23. A. Moutaouaffiq, M. Belhajji, A. Rjeb, S. Sayouri, D.S. Houssaini, and T.D. Lamcharfi, J. Ceram. Process. Res. 23[5] (2022) 570-582.
24. S. Li, Y. Tian, Y. Gao, M. Wang, and P. Liu, J. Xinyang Norm. Univ. (Nat. Sci. Ed.) 35 (2022) 280-284.
25. P. Ren, Y. Wang, A.I. Waidha, O. Clemens, K.V. Lalitha, J. Mater. Chem. C 8 (2020) 8613-8621.
26. Y. Tian, M. Ma, S. Li, J. Dong, G. Mu, and J. Wang, J. Xinyang Norm. Univ. (Nat. Sci. Ed.) 36 (2023) 208-212.
27. A. Molak, A. Winiarski, A.Z. Szeremeta, D.K. Mahato, J. Macutkevic, I. Gruszka, S. Miga, J. Koperski, E. Palaimiene, S. Pawlus, J. Alloy. Compd. 856 (2021) 158216.
28. S. Uddin, A. Zaman, I. Rasool, S. Akbar, M. Kamran, N.

Mehboob, A. Ali, A. Ahmad, M.F. Nasir, and Z. Iqbal, J. Ceram. Process. Res. 21[6] (2020) 745-750.
29. W. Peng, L. Li, S. Yu, P. Yang, and K. Xu, Ceram. Int. 47[20] (2021) 29191-29196.
30. B.N. Parida, P.R. Das, R. Padhee, D. Suara, A. Mishra, J. Rout, and R.N.P. Choudhary, Mater. Res. Bull. 61 (2015) 544-550.
31. Y. Tian, S. Li, B. Zhang, Y. Gong, P. Liu, X. Hu, and Q. Jing, J. Ceram. Process. Res. 23[4] (2022) 430-435.
32. K. Roleder, I. Franke, A.M. Glazer, P.A. Thomas, S. Migal, and J. Suchanicz, J. Phys.-Condens. Mat. 14 (2002) 5399.
33. Z. Li, J. Wu, D. Xiao, J. Zhu, and W. Wu, Acta Mater. 103 (2016) 243-251.
34. N.V. Thinh, L.D. Vuong, D.V. On, T.V. Chuong, L.V.T. Son, T.N. Dat, L.V.T. Son, and V.T. Tung, J. Ceram. Process. Res. 24[3] (2023) 478-485.
35. A. Jain, Y.G. Wang, N. Wang, Y. Li, and F.L. Wang, Ceram. Int. 46[6] (2020) 7576-7585.
36. Y. Tian, L. Cao, Y. Zhang, Y. Jing, X. Ji, Y. Gong, S. Sun, and Q. Jing, Ceram. Int. 46 (2020) 10040-10047.
37. J.H. Kim, K.W. Chae, and C.I. Cheon, J. Ceram. Process. Res. 23[5] (2022) 679-684.
38. Y. Saito, H. Takao, T. Tani, T. Nonoyama, K. Takatori, T. Homma, T. Nagaya, and M. Nakamura, Nature 432 (2004) 84-87.
39. X. Li, J. Fu, Y. Yang, Z. Li, W. Song, and R. Zuo, J. Mater. Sci. 57 (2022) 10233-10241.